

The figure of merit of thermoelectric materials is defined as follows: $ZT = S^2\sigma/k$, where S , σ , and k represent Seebeck coefficient, electrical conductivity and thermal conductivity, respectively. Since the ZT value of the current materials is too low for cost-effective applications, various efforts have been made to improve it. The concept of phonon-glass electron-crystal (PGEC) was proposed and has become a general guideline for developing new thermoelectric materials [2]. In order to obtain the PGEC materials, the idea of complex structure was put forward which imagines a material with distinct regions providing different functions [1]. It is believed that the ideal thermoelectric material would have regions of the structure composed of a high-mobility semiconductor that provides the electron-crystal electronic structure, interwoven with a phonon-glass. The phonon-glass region would be ideal for housing dopants and disordered structures without disrupting the carrier mobility in the electron-crystal region [1].

Based on the above ideas, a series of misfit layer compounds of composition $(MS)_{1+x}(\text{TiS}_2)_2$ ($M = \text{Pb, Bi, Sn}$) are investigated here. They consist of an alternating stacking of CdI_2 -type TiS_2 trigonal anti-prismatic layers and rock-salt-type MS slabs, which could be viewed as a natural superlattice [3]. The TiS_2 layer can provide thermopower as well as electron pathway, according to Imai's research on TiS_2 single crystals [4]. The MS layer was intercalated into the gap of the TiS_2 to form a modulated structure which would suppress the transport of phonons by the interaction between the MS layer and TiS_2 layer and/or disruption of the periodicity of TiS_2 in the direction perpendicular to the layers. The structure and physical properties of misfit layer compounds have been intensively investigated in the 1990s [3,5,6]. In the present study, the thermoelectric performance of these compounds was examined.

2. Results and Discussion

2.1. Crystal structure and XRD patterns

Generally, the crystal structure of $(MS)_{1+x}(\text{TiS}_2)_2$ is composed of a layer of MS sandwiched between two TiS_2 layers with a van der Waals gap [3]. The crystal structure of $(\text{PbS})_{1.18}(\text{TiS}_2)_2$ has been refined from XRD data [7] and is shown in Figure 1. The Pb and S(1) atom of the PbS subsystem are in 4(*i*) sites of space group $C2/m$; each Pb atom is coordinated by five S atoms located at the corners of a slightly distorted square pyramid (NaCl structure type). As Pb atoms protrude from the sulfur planes on both sides, each Pb atom is also bonded to two or three S atoms of the TiS_2 slabs by weak covalent force. The atoms of the $(\text{TiS}_2)_2$ subsystem are on 2(*e*) sites of space group $C2_1/m$. Each Ti atom is coordinated by six S atoms in a trigonal antiprismatic arrangement. The $(\text{TiS}_2)_2$ slab is slightly distorted compared with 1*T*- TiS_2 , in which Ti is octahedrally coordinated. It is seen that the stacking of the two adjacent TiS_2 sandwiches are the same as in 1*T*- TiS_2 .

The XRD patterns of the surfaces of the $(MS)_{1+x}(\text{TiS}_2)_2$ sintered bodies perpendicular to the pressing direction are shown in Figure 2. Sharp (0 0 *l*) peaks which correspond to the planes perpendicular to the *c*-axis can be observed and very few (*h k l*) planes are detected, showing that the *c*-axes are preferentially oriented along the pressing direction. The atomic bondings in these misfit layer compounds are highly anisotropic, and the atomic bondings within the layers must be strong due to high covalency and the interlayer bonding formed mainly by van der Waals force is very weak. Under

the pressure during SPS sintering, the crystals tend to slide along the layers and deflect until the layers become aligned perpendicular to the pressure, thereby resulting in high preferred-orientation of the (0 0 *l*) planes. Rocking curve is also measured to characterize the degree of preferred orientation. It shows that the full width at half maximum (FWHM) of the (0 0 12) peak of $(\text{BiS})_{1.18}(\text{TiS}_2)_2$, $(\text{SnS})_{1.2}(\text{TiS}_2)_2$ and $(\text{PbS})_{1.18}(\text{TiS}_2)_2$ are 17.6° , 15.1° and 17.2° respectively. Although the values are not as low as those of the films, the degree of preferred orientation for the (0 0 *l*) planes of these polycrystalline samples is high enough to approach the in-plane transport prosperities of a single crystal. There are some minor peaks between 20° – 30° in $(\text{PbS})_{1.18}(\text{TiS}_2)_2$ and $(\text{SnS})_{1.2}(\text{TiS}_2)_2$, which may have arisen from the stage-1 compounds $(\text{PbS})_{1.18}\text{TiS}_2$ and $(\text{SnS})_{1.2}\text{TiS}_2$, but their presence should have little influence on the thermoelectric properties because their content is negligible.

Figure 1. Crystal structure of $(\text{PbS})_{1.18}(\text{TiS}_2)_2$ along the incommensurate direction.

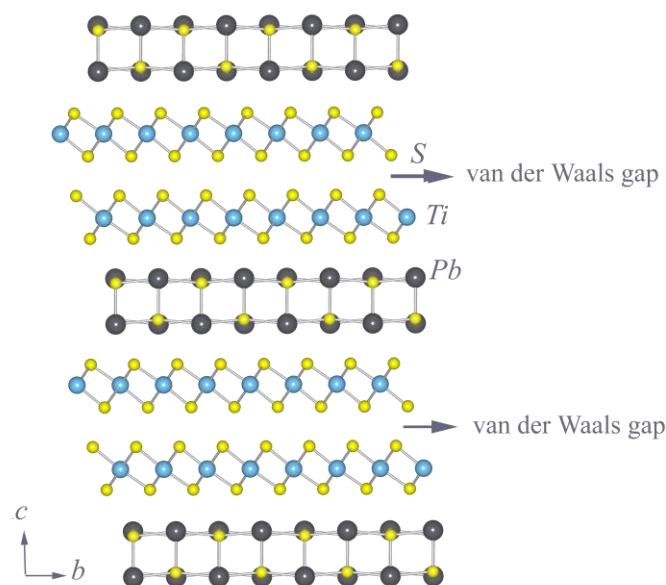
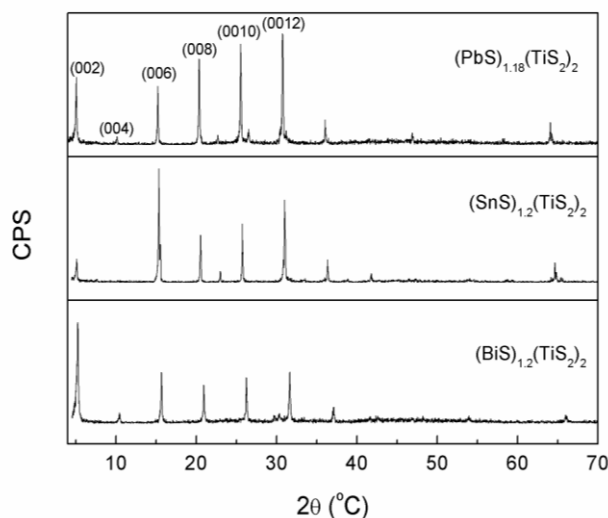


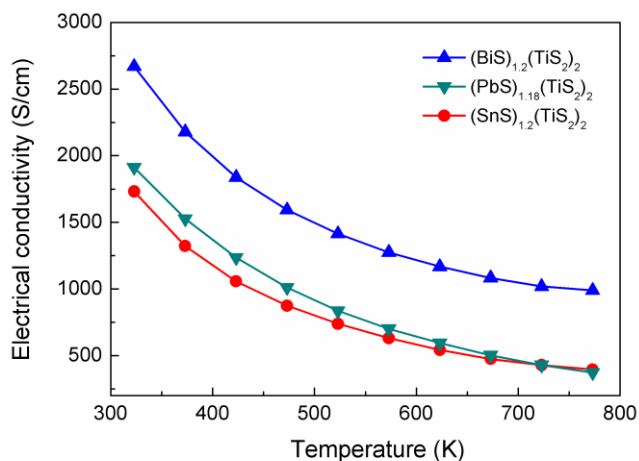
Figure 2. XRD patterns of $(\text{BiS})_{1.2}(\text{TiS}_2)_2$, $(\text{SnS})_{1.2}(\text{TiS}_2)_2$ and $(\text{PbS})_{1.18}(\text{TiS}_2)_2$.



2.2. Electrical properties

As shown in Figure 3, all the $(\text{BiS})_{1.2}(\text{TiS}_2)_2$, $(\text{SnS})_{1.2}(\text{TiS}_2)_2$ and $(\text{PbS})_{1.18}(\text{TiS}_2)_2$ compounds show metallic electrical conductivities of the order of 1,700~2,700 S/cm at room temperature. The electrical conductivity decreases in the sequence of Bi, Pb, Sn for $(\text{MS})_{1+x}(\text{TiS}_2)_2$ over the whole temperature range.

Figure 3. Electrical conductivities of $(\text{BiS})_{1.2}(\text{TiS}_2)_2$, $(\text{SnS})_{1.2}(\text{TiS}_2)_2$ and $(\text{PbS})_{1.18}(\text{TiS}_2)_2$.



The electrical conductivity of materials is determined by the carrier concentration and mobility. Hall measurement was performed to analyze the electron transport properties in these misfit layer compounds. The Hall coefficients are all negative, showing that the dominant carriers in these compounds are electrons. As shown in Figure 4, all the compositions show high carrier concentrations which are almost temperature independent, supporting the metallic conduction mechanism. For the $(\text{MS})_{1+x}(\text{TiS}_2)_2$ compositions, the carrier concentration decreases in the sequence of Bi, Sn, Pb which is consistent with the tendency of electrical conductivity. It has been known that pure TiS_2 is a small-bandgap semiconductor and the carrier concentration is $2.8 \times 10^{20} \text{ cm}^{-3}$ at room temperature [4]. Since the misfit layer compound can be viewed as composite lattice of the MS layer and the TiS_2 layer, the large carrier concentrations of the misfit layer compounds are believed to originate from electron transfer from the MS layer to the TiS_2 layer [3]. From the carrier concentrations and the lattice parameters, we can estimate the number of electrons per Ti atom received for $(\text{BiS})_{1.2}(\text{TiS}_2)_2$, $(\text{SnS})_{1.2}(\text{TiS}_2)_2$ and $(\text{PbS})_{1.18}(\text{TiS}_2)_2$ is 0.45, 0.16 and 0.2, respectively. Much more electron transfer takes place in $(\text{BiS})_{1.2}(\text{TiS}_2)_2$ than the other two compositions, because the valence of bismuth is 3+ here and one can easily deduce that one electron can be transferred from one BiS layer to two TiS_2 layers, leading to that each Ti atom receive 0.6 electrons, which is in reasonable agreement with the above estimation.

The Hall mobilities for the $(\text{MS})_{1+x}(\text{TiS}_2)_2$ compositions are plotted in Figure 5. The mobilities for all the compositions have temperature dependences proportional to $T^{-1.5}$, showing that the electrons are mainly scattered by acoustic phonons. The degree of orientation of the $(0\ 0\ l)$ planes in these polycrystalline samples may affect the mobility, as the electron mobility is much lower in the cross-

plane direction of these misfit layer compounds [8]. However, the similar FWHM of the rocking curve shows that the degree of orientation is close for these three compositions and its effect on the mobility is limited.

Figure 4. Carrier concentrations of $(\text{BiS})_{1.2}(\text{TiS}_2)_2$, $(\text{SnS})_{1.2}(\text{TiS}_2)_2$ and $(\text{PbS})_{1.18}(\text{TiS}_2)_2$.

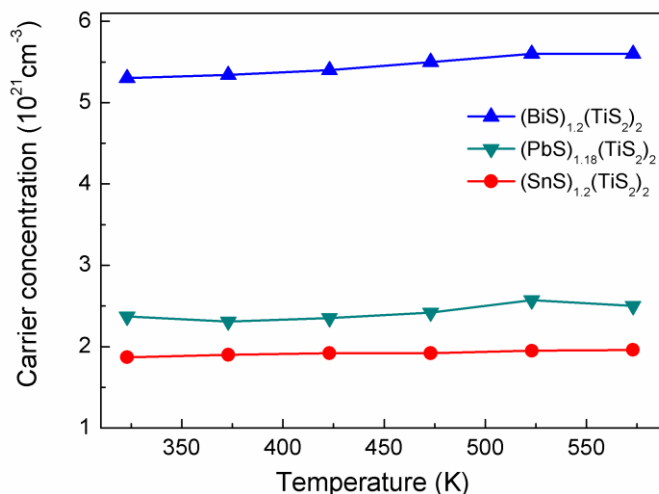
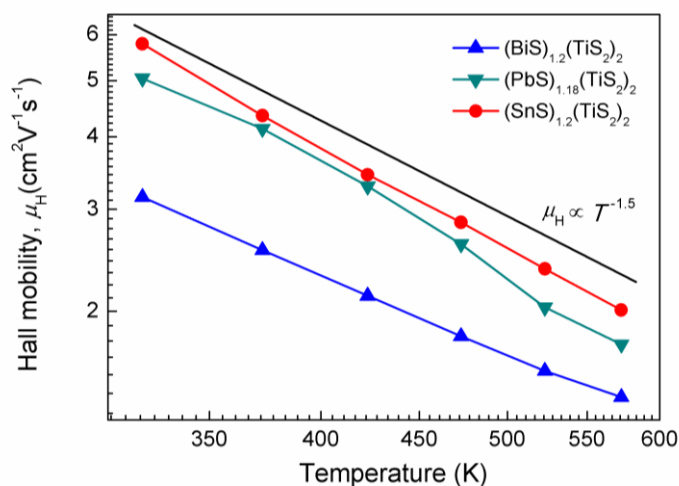


Figure 5. Hall mobilities for $(\text{BiS})_{1.2}(\text{TiS}_2)_2$, $(\text{SnS})_{1.2}(\text{TiS}_2)_2$ and $(\text{PbS})_{1.18}(\text{TiS}_2)_2$.

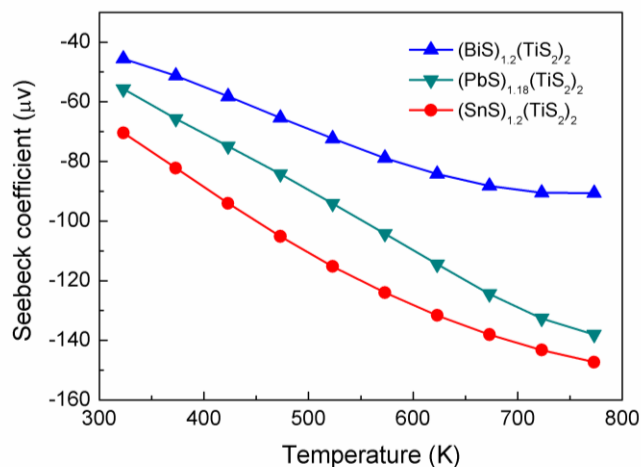


The mobility in the $(\text{MS})_{1+x}(\text{TiS}_2)_2$ decreases in the order of $\text{Sn} > \text{Pb} > \text{Bi}$ which is almost opposite to that of carrier concentration. The electron transfer from the MS layers to the TiS_2 layers may also change the effective mass, resulting in different mobilities. An estimation of the effective mass will be shown below.

The $(\text{MS})_{1+x}(\text{TiS}_2)_2$ compositions show a relatively large Seebeck coefficient, as shown in Figure 6. It can also be seen that the absolute Seebeck coefficient decreases in the order of $\text{Sn} > \text{Pb} > \text{Bi}$. In these intercalation compounds, electrical properties can be described by a rigid band model, which means that the only change in the electronic structure of the host is a change in a degree of band filling due to electron donation from the intercalated species to the host [9]. It is realized that the d orbitals of Ti

plays an important role in determining the physical properties of TiS₂-based materials and the degree of band filling, their energy levels and the width of the *d*-band significantly affect their thermoelectric properties [9]. Accordingly, the Seebeck coefficient decreasing in the order of Sn>Pb>Bi strongly suggests an increase in the number of electrons per Ti atom received, namely indicating higher degree of band filling was achieved.

Figure 6. Seebeck coefficients of (BiS)_{1.2}(TiS₂)₂, (SnS)_{1.2}(TiS₂)₂ and (PbS)_{1.18}(TiS₂)₂.



The density-of-states (DOS) effective mass, m^* , one of the main factors determining S , were estimated by the use of the following equations [10]:

$$m^* = \frac{h^2}{2k_B T} \left[\frac{n_e}{4\pi F_{1/2}(\xi)} \right]^{2/3} \quad (1)$$

where h , k_B , n_e , F_n and ξ are the Plank constant, the Boltzmann constant, the carrier concentration, the Fermi integral, and the chemical potential, respectively. $F_n(\xi)$ and S can be expressed as [10]:

$$F_n(\xi) = \int_0^\infty \frac{x^n}{1 + e^{x-\xi}} dx \quad (2)$$

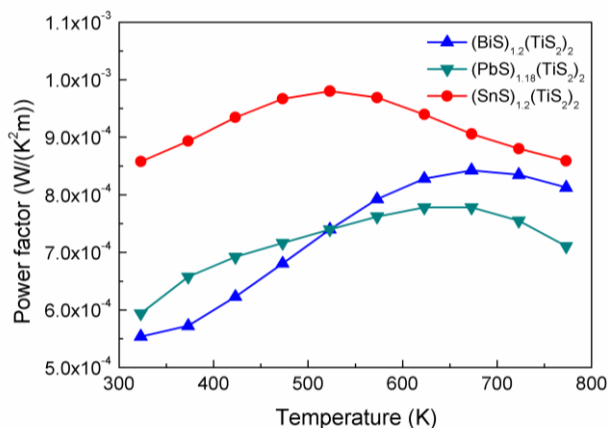
$$S = -\frac{k_B}{e} \left[\frac{(r+2)F_{r+1}(\xi)}{(r+1)F_r(\xi)} - \xi \right] \quad (3)$$

where e is the electron charge, and r is the carrier scattering parameter of relaxation time which was assumed to be $r = 0$ since the carriers are scattered only by acoustic phonons. The m^* values for (BiS)_{1.2}(TiS₂)₂, (SnS)_{1.2}(TiS₂)₂ and (PbS)_{1.18}(TiS₂)₂ were calculated to be $6.3 m_0$, $4.8 m_0$ and $4.5 m_0$, respectively, where m_0 is the bare electron mass. It can be seen that (BiS)_{1.2}(TiS₂)₂ has the highest effective mass, resulting in the lowest mobility as shown in Figure 5.

As shown in Figure 7, the power factors of the (MS)_{1+x}(TiS₂)₂ compositions fall within the range of 5×10^{-4} to 10^{-3} W/K²m, which is much lower than the conventional thermoelectric material Bi₂Te₃ ($\sim 5 \times 10^{-3}$ W/K²m). At lower temperatures, the power factors almost increase in the order of Bi < Pb < Sn, indicative of increased carrier concentration. Although the carrier concentration in (MS)_{1+x}(TiS₂)₂ is not yet optimized, it can be expected that further reduction in carrier concentration

would increase the power factor. Acceptor doping may be employed to reduce the carrier concentration as in the case of TiS_2 doped with Mg and Cd [11,12].

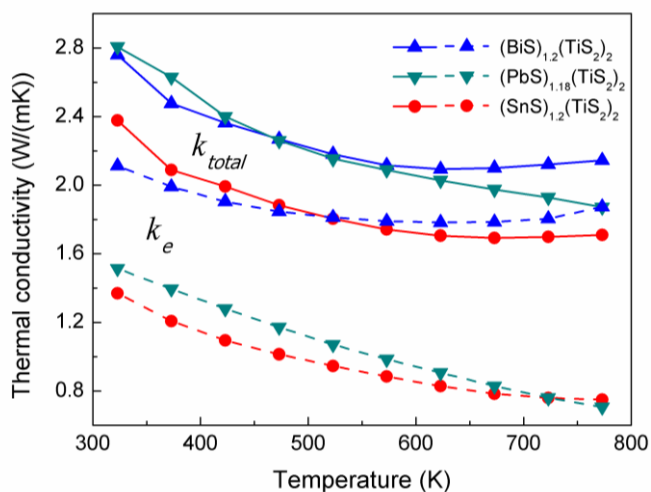
Figure 7. Power factors of $(\text{BiS})_{1.2}(\text{TiS}_2)_2$, $(\text{SnS})_{1.2}(\text{TiS}_2)_2$ and $(\text{PbS})_{1.18}(\text{TiS}_2)_2$.



2.3. Thermal conductivity

As shown in Figure 8, the $(\text{MS})_{1+x}(\text{TiS}_2)_2$ compositions exhibit relatively low thermal conductivity. $(\text{SnS})_{1.2}(\text{TiS}_2)_2$ has lower thermal conductivity than the other compositions in the whole temperature range. Since the thermal conductivity comes from two sources: (1) electrons and holes transporting heat (k_e) and (2) phonons travelling through the lattice (k_l), the electronic thermal conductivity (k_e) is directly related to the electrical conductivity through the Wiedemann-Franz law: $k_e = L_0 T \sigma$, where the Lorenz number L_0 is $2.44 \times 10^{-8} \text{ J}^2 \text{ C}^{-2} \text{ K}^{-2}$. The values of k_e of these $(\text{MS})_{1+x}(\text{TiS}_2)_2$ compositions were calculated and plotted in Figure 8. It can be seen that k_e largely contributes to the total thermal conductivity, especially in $(\text{BiS})_{1.2}(\text{TiS}_2)_2$. $(\text{SnS})_{1.2}(\text{TiS}_2)_2$ has the lowest carrier concentration and electrical conductivity, resulting in the lowest k_e and also the lowest k_{total} .

Figure 8. Total thermal conductivities (k_{total} , solid line) and electron thermal conductivities (k_e , dashed line) of $(\text{BiS})_{1.2}(\text{TiS}_2)_2$, $(\text{SnS})_{1.2}(\text{TiS}_2)_2$ and $(\text{PbS})_{1.18}(\text{TiS}_2)_2$.

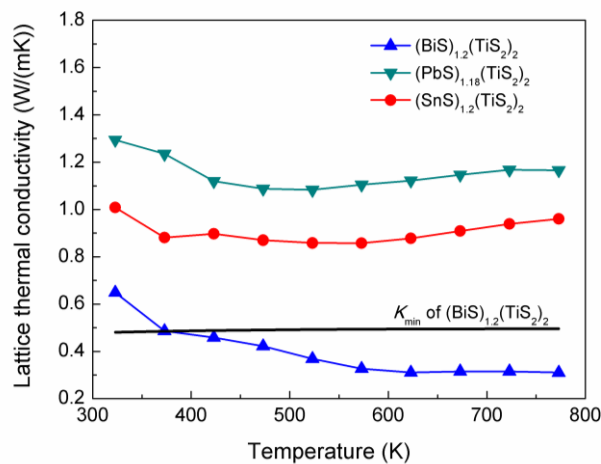


The lattice thermal conductivity was then calculated by subtracting k_e from k_{total} , which is shown in Figure 9. It can be noticed that $(MS)_{1+x}(TiS_2)_2$ has extremely low lattice thermal conductivity, which can be related to their modulated structure. $(BiS)_{1.2}(TiS_2)_2$ exhibits the lowest k_l and can even reach 0.3 W/mK around 700K. The minimum thermal conductivity can be calculated for this composition from the equation [13]:

$$k_{min} = \left(\frac{\pi}{6}\right)^{1/3} k_B n^{2/3} \sum_i v_i \left(\frac{T}{\theta}\right)^2 \int_0^{\theta_i/T} \frac{x^3 e^x}{(e^x - 1)^2} dx \quad (4)$$

The sum is taken over the three sound modes including two transverse and one longitudinal modes with the speed of sound v_i . θ_i is the Debye temperature for each polarization, $\theta_i = v_i(\hbar/k_B)6\pi^2 n)^{1/3}$, where n is the number density of atoms [13]. Using the measured values of V_L, V_{T1}, V_{T2} , the k_{min} was calculated and shown in Figure 9. k_l of $(BiS)_{1.2}(TiS_2)_2$ is even lower than k_{min} , which can hardly be observed in the bulk materials.

Figure 9. Lattice thermal conductivities of $(BiS)_{1.2}(TiS_2)_2$, $(SnS)_{1.2}(TiS_2)_2$ and $(PbS)_{1.18}(TiS_2)_2$. The calculated minimum thermal conductivity for $(BiS)_{1.2}(TiS_2)_2$ is also included.



To analyze the ultra-low thermal conductivity, the kinetic theory of thermal conductivity was used:

$$k=1/3C_v lV \quad (5)$$

where C_v, l and V represent the heat capacity, phonon mean free path and speed of sound, respectively. The heat capacity makes limited contribution to the low thermal conductivity, as the heat capacity approaches $3k_B$ per atom at temperatures higher than the Debye temperature, according to the Dulong-Petit law. The phonon mean free path is restricted by various phonon scattering processes. The present study focused on the the sound velocity which is determined by the density and the elastic constant of a solid. The sound velocity has three polarizations, including one longitudinal mode and two transverse modes, as shown in Figure 10.

A pulse-echo method was used to measure these sound velocities with a 30 MHz longitudinal transducer and a 20 MHz transverse transducer. The measured values are listed in Table 1. The corresponding values for TiS_2 are also included for comparison.

Figure 10. Schematic illustration of the longitudinal and transverse sound velocities of the layered $(MS)_{1+x}(\text{TiS}_2)_2$ compounds.

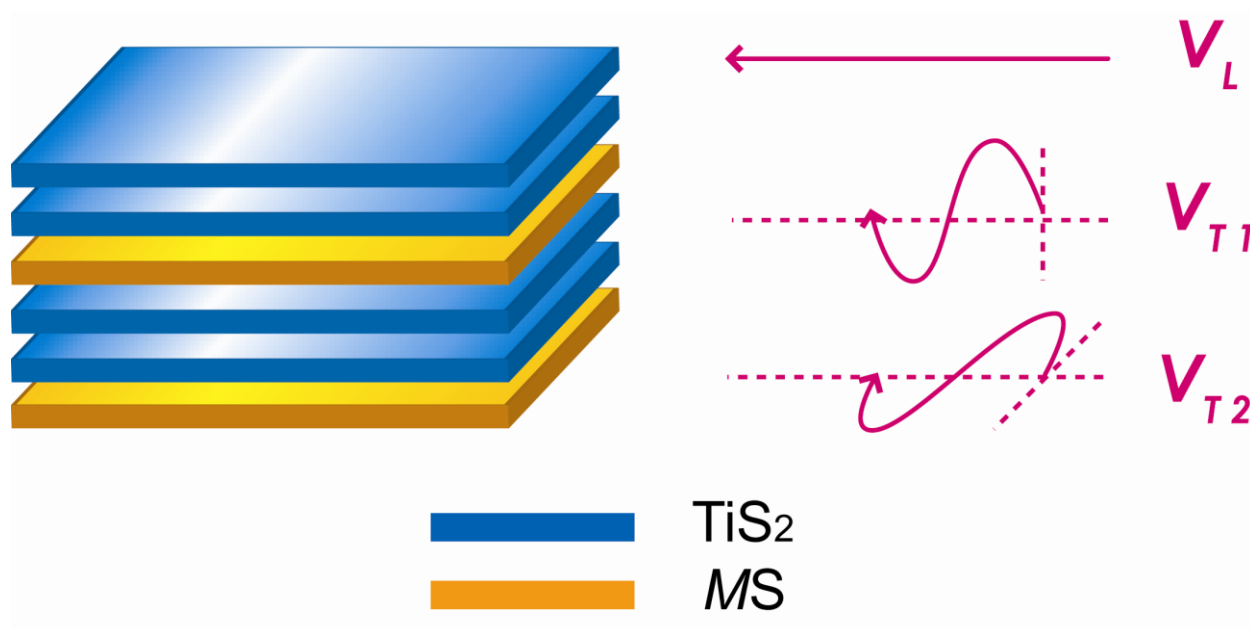


Table 1. Densities, longitudinal and transverse sound velocities, and shear moduli of TiS_2 , $(\text{BiS})_{1.2}(\text{TiS}_2)_2$, $(\text{SnS})_{1.2}(\text{TiS}_2)_2$ and $(\text{PbS})_{1.18}(\text{TiS}_2)_2$.

Material	ρ g/cm ³	V_L m/s	V_{T1} m/s	V_{T2} m/s	G_1 GPa	G_2 GPa
TiS_2	3.21	5284	2799	3295	25.0	34.7
$(\text{BiS})_{1.2}(\text{TiS}_2)_2$	4.57	3662	1350	1688	8.3	13.0
$(\text{PbS})_{1.18}(\text{TiS}_2)_2$	4.69	3834	1120	1837	5.9	15.8
$(\text{SnS})_{1.2}(\text{TiS}_2)_2$	3.87	4111	1578	2352	9.6	21.4

Compared with pure TiS_2 , the longitudinal velocities of the misfit layer compounds are a little decreased, which can be attributed to the increase of density. In contrast, the transverse sound velocities, especially V_{T1} , apparently decreased, which arises from the softening of atomic bonding. The transverse polarization is a kind of shear movement, and the velocity is determined by shear modulus as follows:

$$V_T = \sqrt{\frac{G}{\rho}} \quad (6)$$

where G is the shear modulus and ρ is the density. The shear modulus is calculated by the above equation and shown in Table 1. The shear moduli of the misfit layer compounds are much lower than those of pure TiS_2 due to the intercalation of the MS layers into the TiS_2 layers. It can also be seen that the velocities of the two transverse waves (V_{T1} and V_{T2}) are different, as V_{T1} is mainly determined by the interlayer bonding while V_{T2} is determined by the intralayer bonding. For V_{T1} , the weak interlayer bonding between the MS layer and TiS_2 layer arises either from the electrostatic interaction due to electron transfer between these layers or a weak covalent force between the M atom and the sulfur

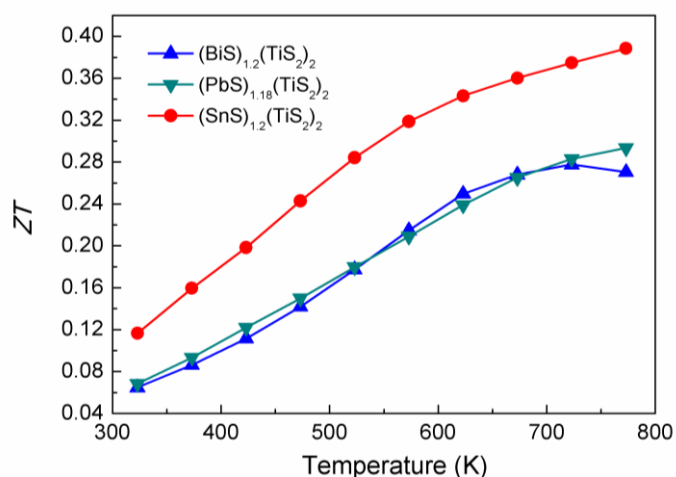
atoms in the TiS_2 layers [14,15]. For V_{T_2} , the intralayer bonding is weakened, possibly due to the incommensurate structure or disruption of periodicity of TiS_2 layers in the direction perpendicular to the layers by the intercalated MS layers.

It has been shown that the sound velocity decreased in the misfit layer compounds due to the weakened bonding, which can partially account for their low thermal conductivity. However, further investigation is required to understand the compositional dependence of lattice thermal conductivity of the $(MS)_{1+x}(\text{TiS}_2)_2$ compounds, which mainly differ in phonon mean free path. It is anticipated that the electron transfer may play a role in determining the phonon transport, because $(\text{BiS})_{1.2}(\text{TiS}_2)_2$ which has the most electron transfer exhibits the lowest lattice thermal conductivity.

2.4. ZT value

The ZT values of the three misfit layer compounds are shown in Figure 11. These misfit layer compounds show an intermediate ZT value of 0.28~0.37 at 700 K. The $(\text{SnS})_{1.2}(\text{TiS}_2)_2$ compound shows the highest ZT value among the three investigated composition and can be considered as promising medium-temperature n -type thermoelectric materials, as it is composed of non-toxic, non-hazardous and naturally abundant elements. Since these misfit layer compounds have extremely low thermal conductivity and rather high carrier concentration, the reduction in carrier concentration can reduce the electronic thermal conductivity and optimize the power factor simultaneously, and much higher ZT value can be expected to be achieved.

Figure 11. ZT values of $(\text{BiS})_{1.2}(\text{TiS}_2)_2$, $(\text{SnS})_{1.2}(\text{TiS}_2)_2$ and $(\text{PbS})_{1.18}(\text{TiS}_2)_2$.



3. Experimental Section

The $(MS)_{1+x}(\text{TiS}_2)_2$ ($M = \text{Bi}, \text{Sn}, \text{Pb}$) powders were prepared using a solid-liquid-vapor reaction method [16,17]. For each composition, the M , S , Ti powders were mixed in the molar ratio of 1:2:5 and then sealed in an evacuated silica tube. The silica tube was then fired in an electric furnace at 500 °C for 12 h, then at 800 °C for 48 h and finally cooled down to room temperature. The obtained powders with luster were ground and sieved. The spark plasma sintering (SPS) method (SPS-1050, Sumitomo Mining Coal Mining Co. Ltd.) was used to densify the powders at 700 °C for 10 min under

the pressure of 50 MPa into a pellet with diameter of 15 mm and thickness of 6 mm. Since the microstructure of the pellet is highly anisotropic, it was deliberately machined for thermoelectric properties measurements in the direction perpendicular to pressure.

The densities of the samples were measured using the Archimedes method. The phase composition was characterized by the X-ray diffraction measurements (RINT-2100, Rigaku). The Seebeck coefficient and electrical conductivity were measured simultaneously by a conventional steady state method and a four-probe method, respectively, in an Ar atmosphere at 300–773 K (RZ-2001K, Ozawa Science). The carrier concentration was determined by Hall effect measurement with a van der Pauw electrode configuration under vacuum of 10^{-3} Pa over the same temperature range (Resi Test 8300, Toyo Technica). The heat capacity and the thermal diffusivity were measured by differential scanning calorimetry (DSC-2910, TA Instruments) and laser-flash method (TC-9000V, ULVAC-RIKO), respectively. The thermal conductivity was calculated as a product of density, heat capacity and thermal diffusivity. The sound velocities including one longitudinal and two transverse modes were measured by the ultrasonic pulse-echo method (Model 5800 PR, Olympus).

4. Conclusions

Thermoelectric properties of a series of misfit layer compounds $(MS)_{1+x}(\text{TiS}_2)_2$ ($M = \text{Pb, Bi, Sn}$) are studied. These compounds appear to be promising for medium-temperature n -type thermoelectric materials. This naturally modulated structure shows low lattice thermal conductivity close to or even lower than the predicted minimum thermal conductivity. Measurement of sound velocities shows that the ultra-low thermal conductivity partially originates from the softening of the transverse modes of lattice wave due to weak interlayer bonding. Meanwhile, electron transfer from the MS layer to the TiS_2 layer deteriorates the thermoelectric performance by reducing the power factor and increasing the electronic thermal conductivity. The SnS intercalation compound $(\text{SnS})_{1.2}(\text{TiS}_2)_2$ has the least electron transfer and the ZT value reaches 0.37 at 700K. Reduction in the carrier concentration in these misfit layer compounds is required to achieve higher ZT value.

Acknowledgements

The authors would like to express their sincere gratitude to Takashi Itoh of the EcoTopia Science Institute (ESI) of Nagoya University for his kind permission to use SPS.

References and Notes

1. Snyder, G.J.; Toberer, E.S. Complex thermoelectric materials. *Nature Mater.* **2008**, *7*, 105-114.
2. Slack, G.A. New Materials and Performance Limits for Thermoelectric Cooling. In *CRC Handbook of Thermoelectrics*; Rowe, D.M., Ed.; CRC Press: Boca Raton, FL, USA, 1995; pp. 407-440.
3. Wiegers, G.A. Misfit layer compounds: Structures and Physical Properties. *Prog. Solid St. Chem.* **1996**, *24*, 1-139.
4. Imai, H.; Shimakawa, Y.; Kubo, Y. Large thermoelectric power factor in TiS_2 crystal with nearly stoichiometric composition. *Phys. Rev. B* **2001**, *64*, 244104.

5. Wiegers, G.A.; Meerschaut, A. Structures of misfit layer compounds $(MS)_nTS_2$ ($M = \text{Sn, Pb, Bi}$, rare earth metals; $T = \text{Nb, Ta, Ti, V, Cr}$; $1.08 < n < 1.23$). *J. Alloy Compd.* **1992**, *178*, 351-368.
6. Rouxel, J.; Meerschaut, A.; Wiegers, G.A. Chalcogenide misfit layer compounds. *J. Alloy Compd.* **1995**, *229*, 144-157.
7. Meerschaut, A.; Auriel, C.; Rouxel, J. Structure determination of a new misfit layer compound $(\text{PbS})_{1.18}(\text{TiS}_2)_2$. *J. Alloy Compd.* **1992**, *183*, 129-137.
8. Wulff, J.; Meerschaut, A.; Van Smaalen, S.; Haange, R.J.; De Boer, J.L.; Wiegers, G.A. Structure, Electrical Transport, and Magnetic Properties of the Misfit Layer Compounds $(\text{PbS})_{1.13}\text{TaS}_2$. *J. Solid State Chem.* **1990**, *84*, 118-129.
9. Meerschaut, A. Misfit layer compounds. *Curr. Opin. Solid St. M.* **1996**, *1*, 250-260.
10. Vining, C.B. A model for the high-temperature transport properties of heavily doped n -type silicon-germanium alloys. *J. Appl. Phys.* **1991**, *69*, 331-341.
11. Qin, X.Y.; Zhang, J.; Li, D.; Dong, H.Z. The effect of Mg substitution for Ti on transport and thermoelectric properties of TiS_2 . *J. Appl. Phys.* **2007**, *102*, 073703.
12. Zhang, J.; Qin, X.Y.; Li, D.; Xin, H.X.; Pan, L.; Zhang, K.X. The transport and thermoelectric properties of Cd doped compounds $(\text{Cd}_x\text{Ti}_{1-x})_{1+y}\text{S}_2$. *J. Alloy. Compd.* **2009**, *479*, 816-820.
13. Cahill, D.G. Lower limit to the thermal conductivity of disordered crystals. *Phys. Rev. B* **1992**, *46*, 6131-6140.
14. C.M., F.; de Groot, R.A.; Wiegers, G.A.; Haas, C. Electronic structure of the misfit layer compounds $(\text{SnS})_{1.2}\text{TiS}_2$: band structure calculations and photoelectron spectra. *J. Phys.: Condens. Mat.* **1996**, *8*, 1663-1676.
15. Ohno, Y. Electronic structure of the misfit-layer compounds PbTiS_3 and SnNbS_3 . *Phys. Rev. B* **1991**, *44*, 1281-1291.
16. Oosawa, Y.; Gotoh, Y.; Onoda, M. Preparation and Characterization of BiM_2X_5 ($M = \text{Ti, Nb, Ta}$; $X = \text{S, Se}$). *Chem. Lett.* **1989**, *18*, 1563-1566.
17. Oosawa, Y.; Gotoh, Y.; Onoda, M. Preparation and Characterization of BiTaS_3 a New layered Ternary Sulfide. *Chem. Lett.* **1989**, *3*, 523-524.

© 2010 by the authors; licensee Molecular Diversity Preservation International, Basel, Switzerland. This article is an open-access article distributed under the terms and conditions of the Creative Commons Attribution license (<http://creativecommons.org/licenses/by/3.0/>).